Measuring In Situ Interfacial Contact Resistance in a Proton Exchange Membrane Fuel Cell

Sigrid Lædre,[1,2,z] Ole Edvard Kongstein,[2] Anders Oedegaard,[3] Frode Seland,[1,*] and Håvard Karoliussen[4]

[1]*Department of Materials Science and Engineering, Norwegian University of Science and Technology, 7491 Trondheim, Norway*
[2]*The Department of Materials and Nanotechnology, SINTEF Industry, 7465 Trondheim, Norway*
[3]*The Department Substainable Energy Technology, SINTEF Industry, 7465 Trondheim, Norway*
[4]*Department of Energy and Process Engineering, Norwegian University of Science and Technology, 7491 Trondheim, Norway*

Interfacial contact resistance (ICR) is one of the remaining hurdles for successful implementation of stainless steel bipolar plates in PEM fuel cells. We have developed a reliable method, using thin gold wires, to measure the interfacial contact resistance between the bipolar plate material and the porous transport layer during fuel cell operation. The ICR values were found to be in the same range as the ICR values measured ex situ after fuel cell operation. Local ex situ ICR measurements on tested plates indicate uneven current distribution during fuel cell operation. Consequently, an average between three measuring points was used for the in situ measurements, which enabled consistent monitoring of the ICR development alongside fuel cell performance. For almost all of the tests, the largest ICR changes took place within the first two hours of operation, showing the importance of early ICR measurements. Non-coated stainless steel and titanium-coated steel BPPs experienced a higher ICR compared to the gold coated stainless steel.
 [DOI: 10.1149/2.1511912jes]

Manuscript submitted January 30, 2019; revised manuscript received June 23, 2019. Published August 7, 2019.

Proton exchange membrane fuel cells (PEMFCs) convert chemical energy to electrical energy, and are predicted to play an important role in the future sustainable society.[1] Even though the first mass produced fuel cell vehicles have entered the market, there are still several durability and economic issues with fuel cells. The main component in a PEMFC is the Membrane Electrode Assembly (MEA), but the Bipolar Plates (BPPs) are essential when connecting several single cells into a stack. In addition to serving as physical separator plates between each individual cell in a stack, these plates assist with water management, cooling, current collection and distribution of fuel and air as well as easy removal of product water.[1,2] In order to serve these functions over the lifetime of a fuel cell stack, the BPPs need to be electrically conducting, corrosion resistant, relatively cheap, easy to produce and both mechanically and chemically stable.[3]

Various sources in the literature have estimated the cost and weight of the BPP in a PEMFC stack,[2,4,5] and even though the numbers vary to some extent, it is clear that the BPP stands for a relatively large part of the total weight and cost. In 2016, the U.S. Department of energy (DOE)[6] updated their targets for bipolar plates for transport applications (Table I). For example, an ambitious ICR target of less than 10 mΩ cm^2[6] by 2020 is put forth.

Carbon-based BPPs have historically been the material of selection in commercially available fuel cells,[7] due to their superior stability and performance in the low pH environment created by the perfluorinated polymer (e.g. Nafion) membrane in PEMFCs.[8] There are, however, incentives to move away from carbon BPPs, as the production of such plates is time-consuming and relatively expensive. Metal bipolar plates are generally cheaper and easier to produce, as they can be stamped instead of formed. Metals possess high electrical- and thermal conductivities, but non-noble metals are prone to degradation in the harsh environment inside a PEMFC stack.[9] When metals corrode, ions are released, which can be detrimental for both catalyst performance and membrane conductivity and longevity. Some metals will also form passive oxides when polarized to more positive potentials, which increases the ICR between the BPP and Gas Diffusion Layer (GDL) in a PEMFC. The high thermal expansion coefficients of common metals can be an issue in PEMFC systems, during start-up and shut-down, where variations in temperature will occur. Various grades of stainless steels have previously been investigated for use as bipolar plate materials.[2,3,10–18] Stainless steels exhibit high mechanical strength, high chemical stability, low gas permeability and are easy to produce into various designs, shapes and sizes.[1,3] In addition, many different stainless steel alloys possessing certain engineered properties exists.

There are several studies described in the literature where interfacial contact resistance of stainless steel has been measured ex situ.[3,19–22] Lee and Lim[19] and Wang et al.[3] used a configuration which estimated the ICR by sandwiching a stainless steel plate between two carbon fiber papers (GDLs) in contact with copper plates in an outer structure. Wang et al.[3] measured an ICR of 50 mΩ cm^2 at 140 N cm^{-2} compaction pressure after polarization at 0.60 V_{SCE} for 60 minutes. Similar results were found when the polarization test duration was altered. Lee and Lim[19] coated the stainless steel with a polymer-based coating containing various amounts of carbon black filler. They measured ICR values between 25 mΩ cm^2 and 850 mΩ cm^2, where high carbon black content resulted in the lowest ICR values. Wang et al.[20] performed ICR measurements on both coated and non-coated stainless steel and reported an ICR of 66.4 mΩ cm^2 at a compaction pressure of 274.4 N cm^{-2}.

Ex situ measurements of ICR between the bipolar plate and other components in the fuel cell have been thoroughly explored in the literature.[3,9,16,19–21,23–32] The literature also describes various models for estimation of ICR in operating fuel cells.[32–39] Even though several attempts have been made to estimate the ICR inside an operating PEMFC, very few studies have been focused on actually measuring this resistance in situ.[25,40–42] There are several advantages with in situ ICR measurements compared to ex situ ICR measurements. By measuring the ICR during fuel cell operation, one can continuously monitor how the ICR develops over time and directly relate this to fuel cell performance and operating conditions, such as humidity level, temperature and gas flow.

The literature describes several works which have focused on both measuring and estimating the current distribution in PEMFCs.[43–48] Alaefour et al.[43] and Noponen et al.[48] used similar methods to study the current distribution through a fuel cell. Current and potential measurements through entire fuel cells can be useful, but they don't provide accurate ICR values between e.g. BPP and GDL within the cell.

Very few studies have been performed where the contact resistance has been measured during fuel cell operation. Most of the ex situ ICR

*Electrochemical Society Member.
[z]E-mail: sigrid.ladre@sintef.no

Table I. Relevant technical targets for bipolar plates for transport applications set by DOE.[6]

Properties	Units	2015 status[a]	2020 targets
Cost[a]	$ kW^{-1}_{net}	7[b]	3
Plate weight	Kg/kW_{net}	<0.4[c]	0.4
Corrosion, anode[d]	$\mu A\ cm^{-2}$	No active peak[e]	<1 and no active
Corrosion, cathode[f]	$\mu A\ cm^{-2}$	<0.1[c]	<1
Electrical conductivity	$S\ cm^{-1}$	<100[g]	>100
Areal specific resistance[h]	$\Omega\ cm^2$	0.006[e]	<0.01

[a]Costs projected to high volume production (500,000 80 kW systems per year), assuming MEA meets performance target of 1,000 mW/cm^2.
[b]Cost when producing sufficient plates for 500,000 systems per year. DOE Hydrogen and Fuel Cells Program Record 15015, "Fuel Cell System Cost—2015." http://www.hydrogen.energy.gov/program_records.html.
[c]C.H. Wang (Treadstone), "Low-cost PEM Fuel Cell Metal Bipolar Plates," 2012 Annual Progress Report, http://www.hydrogen.energy.gov/pdfs/progress12/v_h_1_wang_2012.pdf.
[d]pH 3 0.1ppm HF, 80°C, peak active current $<1 \times 10$–6 A/cm^2 (potentiodynamic test at 0.1 mV/s, −0.4V to +0.6V (Ag/AgCl)), deaerated with Ar purge.
[e]Kumar, M. Ricketts, and S. Hirano, "Ex-situ evaluation of nanometer range gold coating on stainless steel substrate for automotive polymer electrolyte membrane fuel cell bipolar plate," Journal of Power Sources 195 (2010): 1401–1407, September 2009.
[f]pH 3 0.1ppm HF, 80°C, passive current $<5 \times 10$–8 A/cm^2 (potentiostatic test at +0.6V (Ag/AgCl) for >24h, aerated solution.
[g]O. Adrianowycz (GrafTech), "Next Generation Bipolar Plates for Automotive PEM Fuel Cells," 2009 Annual Progress Report, http://www.hydrogen.energy.gov/pdfs/progress09/v_g_2_adrianowycz.pdf.
[h]Includes interfacial contact resistance (on as received and after potentiostatic test) measured both sides per Wang, et al. J. Power Sources 115 (2003) 243–251 at 200 psi (138 N/cm^2).

measurements described in the literature were performed without any gas flow or humidification during fuel cell testing. These measurements are sufficient for initial testing and evaluation of materials and coatings, but they do not provide a comprehensive study of the actual ICR development in an operating fuel cell under realistic conditions. Makkus et al.[42] measured the ICR between the flow plate and the backing at different compaction pressures for Solid Polymer Fuel cell (SPFC) applications, by introducing a thin gold wire between the E-TEK backing plus electrode and the membrane during MEA assembly. They measured the voltage drop between the gold wire and the flow plate and found the ICR to be higher at lower compaction pressures. Ihonen et al.[41] developed a setup for in situ ICR measurements, where potential probes were connected to both the gas backing and current collectors. They show that this configuration enabled reproducible ICR measurements, and that the placement of the probes themselves was crucial.

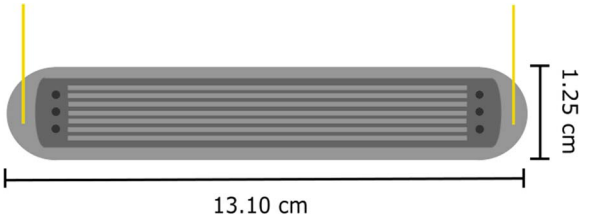

Figure 2. The bipolar plate with parallel flow field. Gold wires were welded to the plate for in situ ICR measurements.

In situ measurements are crucial for understanding the ICR development and its importance on fuel cell performance and degradation. In this work we have developed a modified and improved in situ method based on our original set-up described in reference.[49] Thin gold wires between the BPP and the GDL are introduced to enable in situ interfacial contact resistance measurements. Although the ex situ and in situ values are comparable, local variations prove that careful placement of the gold wires are essential for more reliable in situ measurements. A measurement strategy and comparison between in situ and ex situ measurements are shown and discussed.

Materials and Method Development

The base material for all the tests in this study was AISI 316 stainless steel. The surface area of the plates was 16 cm^2 before the flow field was etched in, and the surface of the non-etched area was 8.059 cm^2.

In situ interfacial contact resistance measurements.—The method used for in situ interfacial contact resistance measurements in this work was based on the set-up given in previous work by Lædre et al.[49] A profile view of this setup is shown in Figure 1, where gold wires (0.025 mm, 99.95%, Goodfellow) are used to measure the ICR between the BPP and the GDL (H23C6, Freudenberg) at the cathode side. A second GDL (H2315 T10A, Quintech) was used at the cathode side to make sure the gold wires were not exposed to the MEA (Gore Primea @ FCM A510.1/MX815.15/C580.4). Figure 2 shows a drawing of the AISI 316L bipolar plates with parallel flow fields that were used in this work. The ICR measurements were limited to the cathode side of the fuel cell, as the complexity of the ICR measuring setup made it difficult to obtain measurements from both anode and cathode in this early prototype. The mounting of the fuel cell with the integrated ICR measuring setup was time consuming, and the number of gold wires placed in between the two GDLs were doubled, to make sure there would be enough viable measuring points.

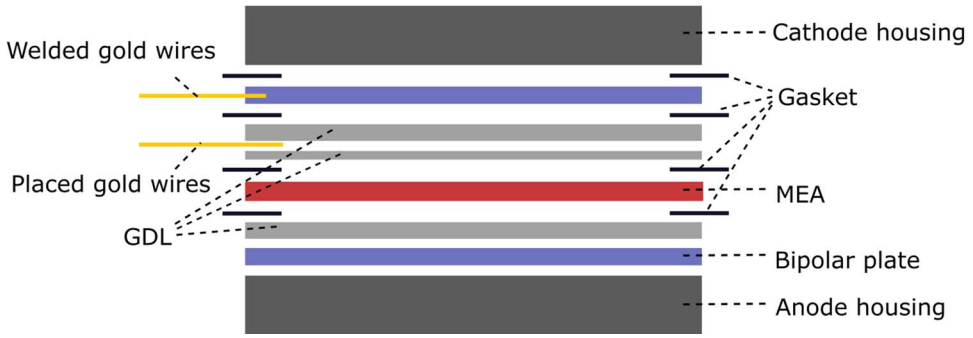

Figure 1. Setup for in situ measurements of ICR as seen from the side with Cathode housing, Gold wires welded to bipolar plate, Gasket (preventing contact between gold wires and other electrically conducting parts of the fuel cell), Gold wires placed in between to sheets of Gas Diffusion layers, Membrane Electrode Assembly, Gas Diffusion Layer, Bipolar plate and Anode housing.

Table II. Parameters used to operate the PEMFC.

Parameter	Value	Parameter	Value
Cell temperature [°C]	75	Conversion synthetic air	0.5
Gas pressure anode [barg]	0.2	Conversion hydrogen	0.67
Gas pressure cathode [barg]	0.3	Compaction pressure [N cm^{-2}]	206
Cell current density [A cm^{-2}]	0.3	Relative Humidity Anode/Cathode [%]	100

One gold wire was point welded to each end of the cathode bipolar plate (Figure 2), in such a way that the gasket covered the wires. This was done to avoid contact between the welded wires and other electrically conductive components in the setup. In addition, three gold wires were placed in between two GDLs. The gold wires were placed near the inlet, middle and outlet of the PEMFC, where approximately 0.5 cm of the wire was in contact with the BPP. The voltage was measured between the gold wires welded to the bipolar plate and the gold wires put in between the two GDLs, resulting in three measured voltages. Note that when the cell was operating, it was tilted so that the flow channels were vertical with inlet on the top and outlet in the bottom. This resulted in one measuring point at the top, one in the middle and one at the bottom of the fuel cell. Welding the gold wires to the plate instead of just placing them on top of the plate ensured that the wires remained where they should throughout the measurements. In addition, the contact resistance only included the oxide on one side of the BPP in addition to the resistance through the GDL.

In addition to the bipolar plate and the two GDLs, two layers of gasket were used on the cathode side of the fuel cell to avoid contact between the individual gold wires and the cell housing. The gold wires were reinforced on the outside of the cell house using conductive tape, and connected to an Agilent 34470A data acquisitions/switch unit. As the ICR was only measured at the cathode side of the fuel cell, only one GDL was needed in addition to the bipolar plate and gaskets at the anode side.

When the fuel cell had been put together, it was mounted into the test station, and wires, tubes and thermocouples were connected to the cell, in order to control the current, gas pressures, humidity and temperature. Compaction pressure over the active cell area was applied by a pneumatic system, and this pressure was kept stable throughout the entire fuel cell operation at approx. 200 N cm^{-2}. The operational parameters that were applied are shown in Table II. A customized LabVIEW program was used to operate the fuel cell, and a Fuel Cell Technologies Inc. humidifier was used to keep a 100% relative humidity of both hydrogen (5.0 Yara Praxair, anode) and air (synthetic air, 5.0 Yara Praxair, cathode) entering the fuel cell. The cell was set to operate under current control for most of the test procedures, and thus the cell voltage varied somewhat throughout the tests.

Table III describes the different fuel cell tests performed during this study. The duration of each test in this study was set to 72 hours, and all the tests were performed on Stainless Steel (316L) BPPs. However, the coating and current/voltage were altered. For three of the tests, open circuit voltage (OCV) was applied for various time intervals. Non-coated BPPs were used during these tests. In addition, gold coated- and titanium coated BPPs were put through the 72 hour test at baseline conditions, defined to be 72 hours at 0.30 A cm^{-2}.

Table III. The tests performed during this study, including material, coating and operational conditions.

Name	Coating	Description
Baseline	none	0.3 A cm^{-2} for 72 hours
OCV 4.2%	none	0.3 A cm^{-2} for 23 hours + 1 hour at OCV*
OCV 16.7%	none	0.3 A cm^{-2} for 50 min + 10 min at OCV*
OCV 50%	none	0.3 A cm^{-2} 30 min + 30 min at OCV*
Gold coating	Gold	0.3 A cm^{-2} for 72 hours
Titanium coating	Titanium	0.3 A cm^{-2} for 72 hours

*The test was cycled between 0.3 A cm^{-2} and OCV for 72 hours.

Ex situ interfacial contact resistance measurements.—A schematic of the ex situ ICR measurement setup is shown in Figure 3. This setup was designed to simulate the structure of a PEMFC, and at the same time make it time efficient to measure the ICR. The setup comprised of two gold coated copper plates, a pneumatic cylinder (Camozzi QP2A080A010) to control compaction pressure by moving the bottom plate and an external power supply (XDL 56-5 DC, Xantex). The test specimen with a GDL (H23C6, Freudenberg) on top was placed in between the two gold coated plates, and a current of 2.0 A was applied. The corresponding voltage between the top gold coated plate and an isolated pressure controlled pin mounted in the center of the bottom gold coated plate was measured with a Fluke 76 true RMS multimeter. The pin was only used for measuring of the voltage, and the ICR was calculated from this voltage by use of Ohm's law. A smaller, point measuring adaption of this ex situ ICR setup was developed and used to measure ICR on small areas (0.6 cm^2) along the length of the BPP.

Results and Discussion

In situ interfacial contact resistance measurements.—The cathode side was chosen for the in situ measurements as it is expected to experience the highest voltages and temperatures, and to accumulate the highest amount of water, which can affect the oxide formation on the BPP and thus the ICR. The recorded cell voltages obtained for each test at 0.3 A cm^{-2} are shown in Figure 4. The voltage transients for continuous operation are similar for the three different materials/coatings and within 30–40 mV of each other with gold coating showing the highest cell voltage. The differences observed can be attributed to the insufficient initial conditioning of the cells. All controls and measurements were initiated at the same time without prior condition. This includes applied current, temperature, humidity and gas flow. This was done in order to obtain ICR values unaffected by any conditioning protocols. For three of the tests the current was set to 0 (OCV) for various periods of time, which explains the voltages close to 0.9 V in Figure 4. For the OCV 4.2%, OCV 16.7% and OCV 50% the cell voltage varies between approx. 0.6 V and 0.9 V, where

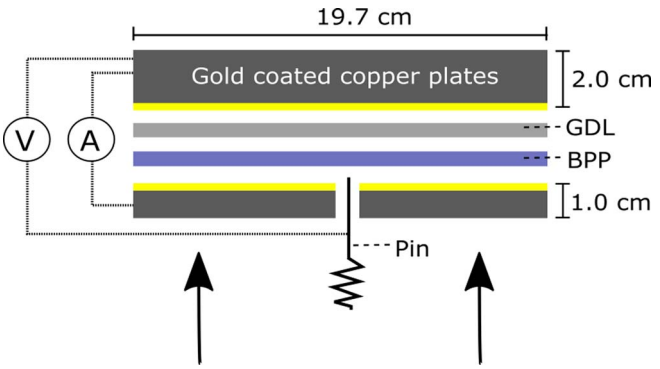

Figure 3. Setup for ex situ ICR measurements with Gold coated copper plates, Gas diffusion layer, Bipolar test plate and spring-loaded pin.

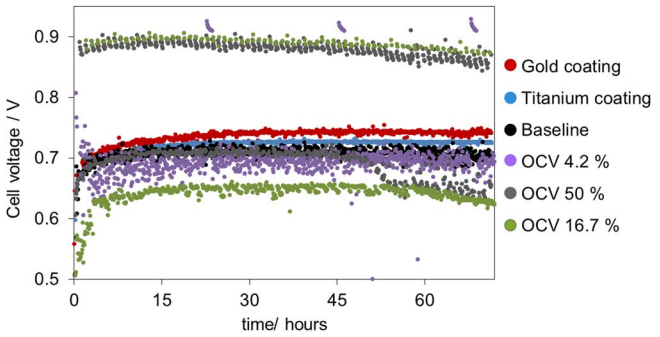

Figure 4. Cell voltages obtained during fuel cell operation for all of the tests in this study.

the lower values are from the 0.3 A cm^{-2} operation, and the higher ones are from the OCV operation. The OCV 4.2% gave higher voltages than both OCV 16.7% and OCV 50% at open circuit, 0 A cm^{-2}. The OCV 4.2% and OCV 50% tests showed similar performances during operation at 0.3 A cm^{-2} and close to the baseline cell voltage for continuous operation. The OCV 16.7% test showed a somewhat lower cell voltage during operation. Interestingly, there is a change in cell voltage at 45 hours which correlates with small changes in OCV and ICR (Figure 5A), but the change in ICR cannot alone explain the change in voltage. This could be due to changes in the state of the MEA.

Figures 5A and 5B displays the development of the interfacial contact resistances with time for each test (see Table III), while Figures 5C and 5D show the same development for the first 5 hours. The ICRs given are the averaged ICR values from the three measuring points in each cell. The test resulting in highest average ICR values is the one where the cell was operated at OCV 50% of the time, with ICR values close to 30 mΩ cm^2 throughout the entire test. The gold coated steel BPP showed the lowest averaged ICR values, approaching 4 mΩ cm^2 with time. This test was the only one resulting in ICR values below DoE's target for ICR at 10 mΩ cm^2.[50] The low ICR values for gold were to be expected, as it does not form a thick non-conducting oxide on its surface. The titanium coated steel BPP showed ICR values between 20 and 25 mΩ cm^2, placing it second highest in Figure 5. At the voltages inside an operating PEMFC, titanium is expected to form a stable oxide (TiO_2), with semiconductor properties.[51] This oxide is thus most likely responsible for the relatively high ICR encountered with the titanium coated plates. The results from the baseline test showed ICR values similar to the OCV 16.7% and the OCV 4.2% tests. Towards the end of the 72 hour operation they were all close to 15 mΩ cm^2 (Figure 5A).

As can be seen in Figure 5B, there is not a common trend for how the ICR developed within the first few hours of operation. One reason for the changes in ICR at the beginning of any test, could be the buildup and/or stabilization of oxides on the surface of the stainless steel. In order to study how the ICR developed from the very beginning of cell operation, gas flow, temperature and humidity were introduced into the cell housing at the same time as the current was set. For the same reason, conditioning was skipped at the beginning of cell operation. All of these factors will affect the oxide formation on the BPP surface, which may explain the instabilities in ICR at the beginning of each test. The pH in the fuel cell will also take some time to stabilize, and thus possibly affect the stability of already formed oxides. It is evident from all of the graphs in Figure 5 that the largest changes in ICR take place within the first hours of operation, confirming the importance of starting the ICR measurements from the very beginning. Another important aspect of fuel cell operation is that the overall performance of the cell can differ from test to test, depending on the MEA performance and the symbiotic effects between all the parameters in an operating fuel cell.

Figure 6 shows three ICR values for each in situ test after 72 hours of operation, one for each measuring point in the cell. As mentioned in In situ Interfacial Contact Resistance Measurements section, the three measuring points were placed on the top (inlet), middle and bottom(outlet) of the cell. The highest of all the ICR values presented in Figure 6 is the one obtained from the bottom measuring point in the 50% OCV test, resulting in an ICR of 62 mΩ cm^2. The measuring

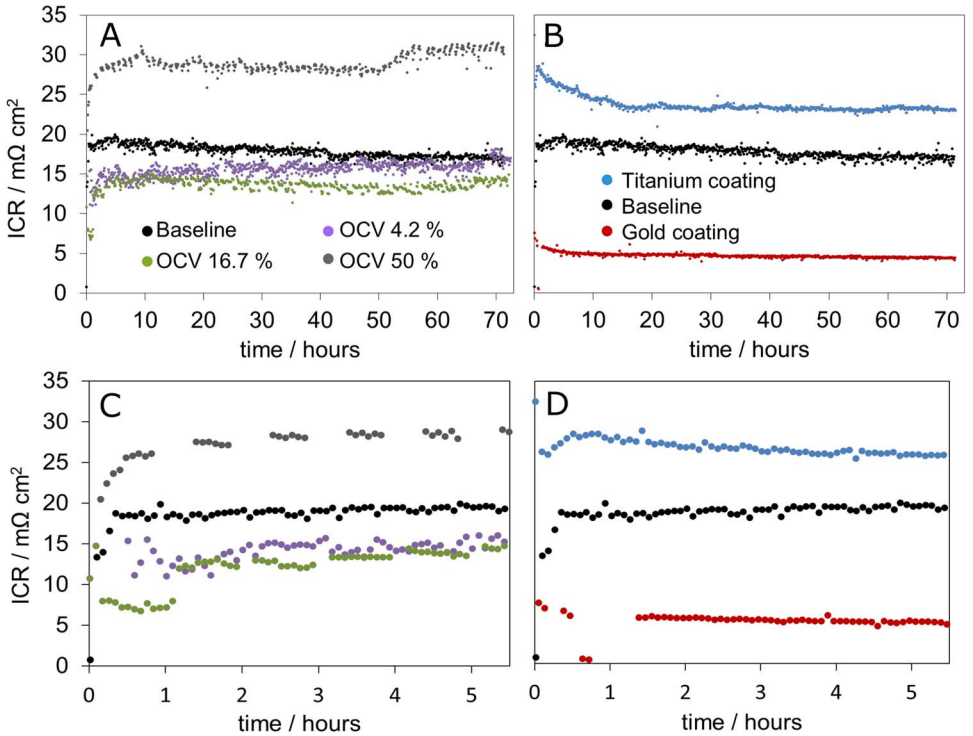

Figure 5. A) ICR obtained for non-coated AISI 316L BPPs when OCV was applied for various durations of time. B) ICR obtained for Gold- and Titanium coated AISI 316L BPPs. C) The first five hours of the graph in Figure A. D) The first five hours of the graph in Figure B.

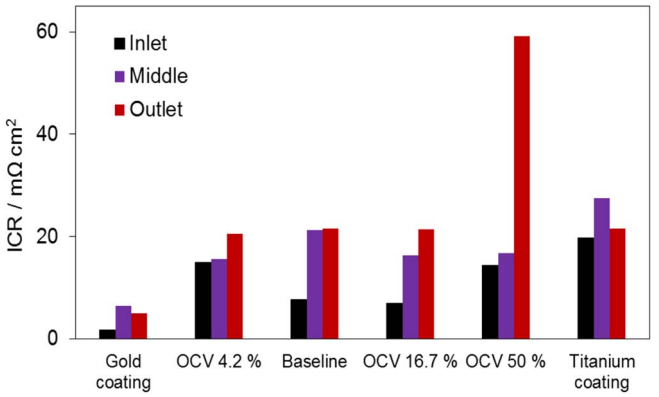

Figure 6. In situ ICR values obtained at three measuring points in the cell after 72 hours fuel cell operation.

point on top of the cell operated at constant current with gold coated steel plates showed the lowest ICR at 2 mΩ cm^2. As a general trend, the ICR obtained from the BPP at the outlet part was higher than at the inlet part. A likely cause for this could be that the area close to the outlet is more prone to mass transport limitations by the water accumulated from both humidification and the reaction at the cathode, and due to the way the cell was placed in the station. Alternatively, it could be a consequence of uneven current distribution across the cell. For all the tests, the ICR obtained from the measuring point close to the inlet is lower than the ICR obtained in the middle and close to the outlet. The values obtained from the point close to the outlet are higher than the other measuring points for all the tests performed on pure AISI 316L steel, whereas for the titanium and gold coated BPPs, the measuring point in the middle showed the highest ICR value. As there are variations in ICR across the BPP surface presumably due to uneven current distribution in the cell, the average ICR may be a better way of displaying the actual ICR.

When comparing OCV 50% to the other OCV tests in Figure 5, one might suggest that operating the fuel cell between OCV and 0.3 A cm^{-2} causes an increase in ICR when the on and off periods are the same (OCV 50%). However, Figure 6 shows a very high ICR at the outlet measuring point as compared to the other two. Even though a higher value is to be expected close to the outlet, the measurement obtained at this point is so much higher than the other two that it may be a measurement artefact. Brightman found the corrosion potential of the bipolar plate to only be weekly coupled to the electrode potential due to the low ionic conductivity of the discontinuous aqueous phase in the GDL,[52] and the operating potential may therefore not play a crucial role for the corrosion potential of the BPP.

Figure 7 shows the development of ICR with time at each measuring point for the baseline test (7A) and OCV 4.2% test (7B). Figures 7C and 7D show the same for the first 5 hours of the test. The ICR at each point was in general found to be rather stable throughout the operation for all samples tested, where the trend is seen to be similar for each measuring point.

Measuring the interfacial contact resistance between the bipolar plate and the gas diffusion layer during fuel cell operating is challenging, as the effects from various parameters can be difficult to separate from one another. Current distribution, water distribution, heat distribution and pH variations throughout the fuel cell will impact the measured ICR. For example, the current distribution in an operating fuel cell will depend strongly on the distribution of reactant gases, hence the (in)homogeneity of fluid flow in the cell. Depending on how ideal the cell design and operating conditions are, measuring the ICR only at one point on the BPP surface would create a very high uncertainty. The authors believe that increasing from one to three measuring points greatly increases the accuracy of the measurements. The bipolar plate used in this work resulted in co-flow arrangement of fuel and synthetic air in the fuel cell (Fig. 2). Alaefour et al.[43] found the current to decrease from approx. 700 mA cm^{-2} to approx. 400 mA cm^{-2} between inlet and outlet in a co-flow arranged fuel cell. The temperature was kept at 65°C and 100% RH. This corresponds well with the generally higher ICR values obtained at the outlet of the fuel cell during this work.

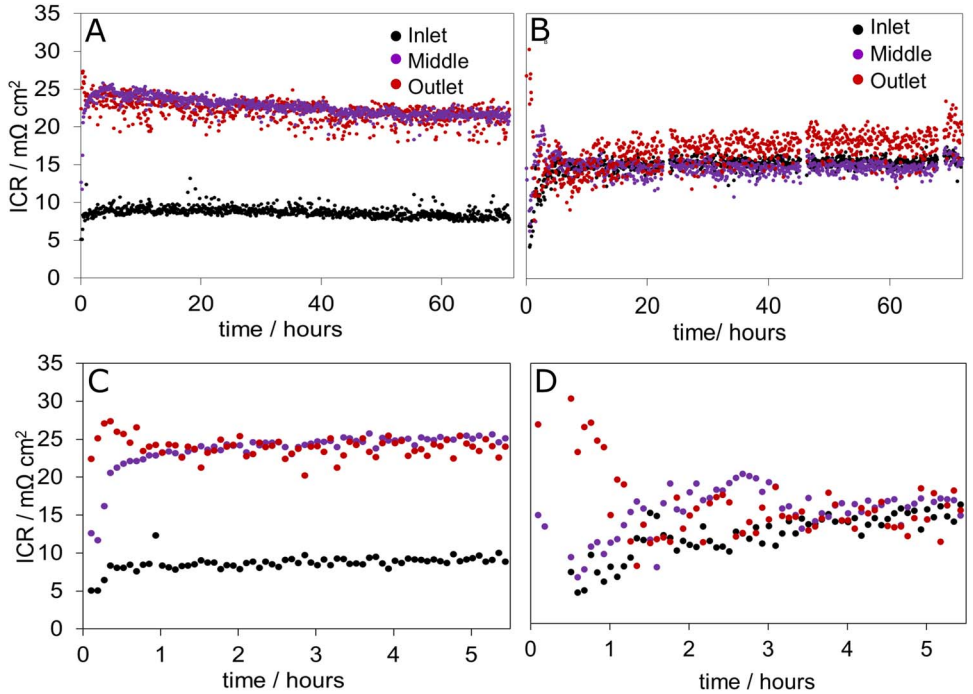

Figure 7. In situ ICR values obtained at inlet, middle and outlet of the fuel cell A) during 72 hours fuel cell operation for the baseline test, B) during 72 hours fuel cell operation for the OCV 4.2% test, C) the first 5 hours of the baseline test, D) the first 5 hours of the OCV 4.2% test.

Table IV. Ex situ ICR measurements performed on five smaller areas of the bipolar plate that had been used on the cathode side during the OCV 50% test.

Measuring point	1	2	3 (middle)	4	5
ICR value [mΩ cm^2]	11.0	10.4	10.0	10.1	9.8

In order to confirm the variation in the in situ ICR across the BPP surface, point measurements were performed ex situ on the BPP from the OCV 50% test (Table IV). Five points were used, where points 1, 3 and 5 were in the same area as the three in situ measuring point. The values presented in Table IV are not comparable to the other measured values presented in this article, as the compaction pressures used in the point measuring setup was much higher (1190 N cm^{-2}). Due to the way this setup was made, it was not possible to get accurate measurements at pressures similar to the ones experienced by the BPP in an operating fuel cell. The OCV 50% BPP was chosen, as it showed the greatest variation between the in situ ICR measuring points. As can be seen from Table IV, there are some variations between the different ex-situ measuring points, but they are small compared to the variations between the in situ measurement points. This emphasizes the possible impact that uneven current distribution may have on ICR measurements, and it is likely to believe that this could be even higher in an operating fuel cell.

Ex situ interfacial contact resistance measurements.—ICR values measured after the in situ tests at various compaction pressures are presented in Figure 8a, while Figure 8b shows the ICR values obtained before and after the in situ tests at 200 N cm^{-2}. The focus of the ex situ ICR in this work was to compare it to the in situ measurements, and the resistance is thus reported without deducting the ICR contribution from the bulk GDL. For stainless steel BPPs, the main contribution to the ICR is expected to come from the oxides formed on the steel surface, and not the GDL.

The ICR values in Figure 8b show that all the materials experienced an increase in ICR during polarization, except for the gold coated stainless steel. This was expected, as there is limited oxide formation on the gold surface. The ICR measured for titanium coated stainless steel before the fuel cell test, was close to twice the values of the bare steel. This plate also obtained the highest ICR value over the entire range of compaction pressures (Fig. 8a) with 25.8 mΩ cm^2 obtained at 200 N cm^{-2} (Fig. 8b). The results from both in situ and ex situ measurements show that the ICR was lowest for gold coated steel. The two tests resulting in highest measured ICR values, were the tests performed with titanium coated BPPs and OCV operation 50% of the time. At high potentials, the BPP is more prone to corrosion and oxide formation, which could result in higher ex situ ICR values for the BPPs that were exposed to OCV over longer periods of time. This could explain why the measured ICR after polarization was higher for the OCV 50% and OCV 16.7% BPPs, compared to the baseline and OCV 4.2% BPPs.

When comparing the ex situ (Figures 8a and 8b) to the in situ ICR values (Figures 5 and 6), it becomes evident that the in situ and ex situ ICR values are all in the same range at approximately 200 N cm^{-2}. The lowest ICR values obtained from both in situ and ex situ measurements were the ones with gold coated stainless steel BPPs, and the ICR values were close to 5 mΩ cm^2 (average in situ) and 6 mΩ cm^2 (ex situ). The highest average ICR values from the in situ measurements were close to 30 mΩ cm^2 (OCV 50%, Fig. 5), while the highest value from the ex situ measurements were 25,8 mΩ cm^2 (titanium coated steel). These results show that the ex situ and in situ ICR values are comparable and that most of the trends seen in situ correlate with the ICR values measured ex situ. Continuous in situ measuring of ICR provides an option for online monitoring and diagnostic tool of the status and performance of BPPs, as well as the interaction between the BPP and the GDL.

Even though most of the ICR values obtained after fuel cell operation in this study were higher than the 10 mΩ cm^2 target set by DoE,[50] they are all in the same order of magnitude. The compaction pressure in this study was a bit higher than the recommended 138 N cm^{-2} (DOE,[6] Table I), but the correlation between in-situ and ex-situ ICR was the main objective here.

Conclusions

The authors have developed a method for in situ ICR measurements, which provides results comparable to the already established ex situ technique. The principle of the method is simple, using thin gold wires to measure the ICR directly between the BPP and the GDL. From the results presented, it can be seen that the average ICR value obtained from three measuring points in situ is in the same range as the ICR value measured ex situ after fuel cell operation. For almost all of the tests, the largest changes in ICR take place within the first hours of operation, which shows that the measurements at the very start of cell operation are very important. The gold coated BPP showed in situ ICR values close to 5 mΩ cm^2, while the ex situ ICR obtained after operation was 7 mΩ cm^2 The highest ICR values obtained from both in situ and ex situ measurements were on the OCV 50%, at approx. 30 mΩ cm^2 and 35 mΩ cm^2, respectively. Trends seen in the in situ (online) values were confirmed by the ex situ measured ICR. Non-coated stainless steel and titanium-coated steel BPPs experienced a higher increase in ICR compared to the gold coated stainless steel.

Ex situ ICR measurements performed on smaller areas of the plates, with a point measuring setup, showed that the variation between the three in situ measuring points were probably caused by uneven current distribution in the cell. The use of three measuring points was thus more accurate than just one. The method developed during this work will be an important tool when evaluating coatings for BPPs in future projects. The accuracy of the measurements are more than good enough for evaluating whether a coating is promising enough for

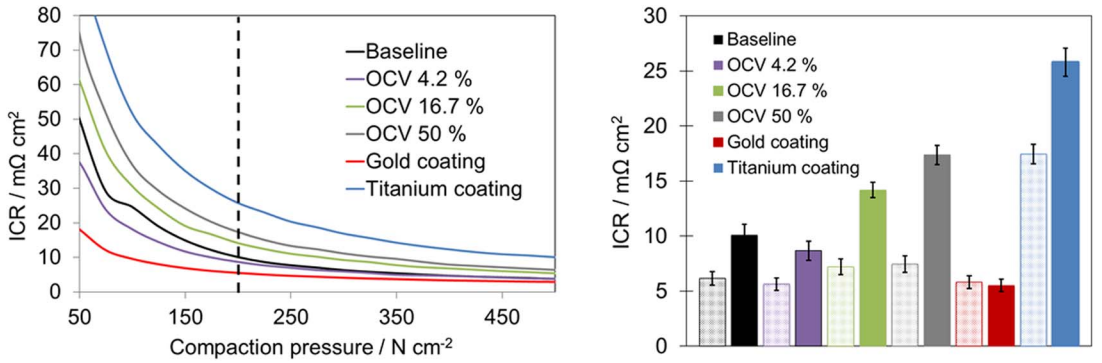

Figure 8. a) Ex situ ICR between GDL and BPP obtained after 72 hours of in situ fuel cell operation as a function of pressure. b) ICR values before (left, dots) and after (right, solid) in situ operation at 200 N cm^{-2}.

further research, but further testing and development of the equipment has already started.

Acknowledgments

The authors would like to thank the Norwegian University of Science and Technology and SINTEF Industry for funding the work described in this article. The STAMPEM and COATELY project are both acknowledged for contributions to this work.

ORCID

Sigrid Lædre https://orcid.org/0000-0002-4234-2979

References

1. A. Hermann, T. Chaudhuri, and P. Spagnol, *International Journal of Hydrogen Energy*, **30**, 1297 (2005).
2. R. A. Antunes, M. C. L. Oliveira, G. Ett, and V. Ett, *International Journal of Hydrogen Energy*, **35**, 3632 (2010).
3. H. L. Wang, M. A. Sweikart, and J. A. Turner, *Journal of Power Sources*, **115**, 243 (2003).
4. H. Tsuchiya and O. Kobayashi, *International Journal of Hydrogen Energy*, **29**, 985 (2004).
5. S. Aalto, P. Kauranen, J. IHONEN, and P. Kosonen, Bipolar plate, method for producing bipolar plate and PEM fuel cell, in, Google Patents (2009).
6. U.S. Department of Energy, *Fuel Cell Technologies Office Multi-Year Research, Development, and Demonstration Plan*, in (2016).
7. R. Taherian, *Journal of Power Sources*, **265**, 370 (2014).
8. D. A. Schiraldi, *Journal of Macromolecular Science, Part C*, **46**, 315 (2006).
9. H. Wang and J. A. Turner, *Fuel Cells*, **10**, 510 (2010).
10. N. D. L. Heras, E. P. L. Roberts, R. Langton, and D. R. Hodgson, *Energy Environ. Sci.*, **2**, 206 (2009).
11. H. Tawfik, Y. Hung, and D. Mahajan, *Journal of Power Sources*, **163**, 755 (2007).
12. Y. Wang and D. O. Northwood, *Electrochimica Acta*, **52**, 6793 (2007).
13. A. M. Lafront, E. Ghali, and A. T. Morales, *Electrochimica Acta*, **52**, 5076 (2007).
14. Y. Yang, L.-J. Guo, and H. Liu, *International Journal of Hydrogen Energy*, **36**, 1654 (2011).
15. S. Lædre, O. E. Kongstein, A. Oedegaard, F. Seland, and H. Karoliussen, *International Journal of Hydrogen Energy*, **37**, 18537 (2012).
16. C. Turan, Ö. N. Cora, and M. Koç, *Journal of Power Sources*, **243**, 925 (2013).
17. J. André, L. Antoni, and J.-P. Petit, *International Journal of Hydrogen Energy*, **35**, 3684 (2010).
18. C. K. Jin, J. Y. Koo, and C. G. Kang, *International Journal of Hydrogen Energy*, **39**, 21461 (2014).
19. Y. B. Lee and D. S. Lim, *Curr. Appl. Phys.*, **10**, S18 (2010).
20. L. Wang, D. O. Northwood, X. Nie, J. Housden, E. Spain, A. Leyland, and A. Matthews, *Journal of Power Sources*, **195**, 3814 (2010).
21. D. D. Papadias, R. K. Ahluwalia, J. K. Thomson, H. M. Meyer Iii, M. P. Brady, H. Wang, J. A. Turner, R. Mukundan, and R. Borup, *Journal of Power Sources*, **273**, 1237 (2015).
22. K. McCay, O. E. Kongstein, A. Oedegaard, A. O. Barnett, and F. Seland, *International Journal of Hydrogen Energy*, **43**, 9006 (2018).
23. J. André, L. Antoni, J.-P. Petit, E. De Vito, and A. Montani, *International Journal of Hydrogen Energy*, **34**, 3125 (2009).
24. C. Turan, Ö. N. Cora, and M. Koç, *International Journal of Hydrogen Energy*, **37**, 18187 (2012).
25. A. Oyarce, N. Holmström, A. Bodén, C. Lagergren, and G. Lindbergh, *Journal of Power Sources*, **231**, 246 (2013).
26. K. Feng, T. Hu, X. Cai, Z. Li, and P. K. Chu, *Journal of Power Sources*, **199**, 207 (2012).
27. A. Miyazawa, T. Himeno, and A. Nishikata, *Journal of Power Sources*, **220**, 199 (2012).
28. M. S. Ismail, D. B. Ingham, L. Ma, and M. Pourkashanian, *Renewable Energy*, **52**, 40 (2013).
29. V. Mishra, F. Yang, and R. Pitchumani, *Journal of Fuel Cell Science and Technology*, **1**, 2 (2004).
30. D. Ye, E. Gauthier, J. B. Benziger, and M. Pan, *Journal of Power Sources*, **256**, 449 (2014).
31. J. Jin, D. Zheng, and H. Liu, *International Journal of Hydrogen Energy*, **42**, 28883 (2017).
32. A. Vikram, P. R. Chowdhury, R. K. Phillips, and M. Hoorfar, *Journal of Power Sources*, **320**, 274 (2016).
33. P. Zhou, C. W. Wu, and G. J. Ma, *Journal of Power Sources*, **159**, 1115 (2006).
34. Y. Zhou, G. Lin, A. J. Shih, and S. J. Hu, *Journal of Power Sources*, **163**, 777 (2007).
35. M. H. Akbari and B. Rismanchi, *Renewable Energy*, **33**, 1775 (2008).
36. X. Lai, D. A. Liu, L. Peng, and J. Ni, *Journal of Power Sources*, **182**, 153 (2008).
37. H. Sadeghifar, N. Djilali, and M. Bahrami, *Journal of Power Sources*, **266**, 51 (2014).
38. L. Zhang, Y. Liu, H. Song, S. Wang, Y. Zhou, and S. J. Hu, *Journal of Power Sources*, **162**, 1165 (2006).
39. P. Liang, D. Qiu, L. Peng, P. Yi, X. Lai, and J. Ni, *Energy Conversion and Management*, **169**, 334 (2018).
40. C. J. Netwall, B. D. Gould, J. A. Rodgers, N. J. Nasello, and K. E. Swider-Lyons, *Journal of Power Sources*, **227**, 137 (2013).
41. J. Ihonen, F. Jaouen, G. Lindbergh, and G. Sundholm, *Electrochimica Acta*, **46**, 2899 (2001).
42. R. C. Makkus, A. H. H. Janssen, F. A. de Bruijn, and R. K. A. M. Mallant, *Journal of Power Sources*, **86**, 274 (2000).
43. I. Alaefour, G. Karimi, K. Jiao, and X. Li, *Applied Energy*, **93**, 80 (2012).
44. M. Noponen, J. Ihonen, A. Lundblad, and G. Lindbergh, *Journal of Applied Electrochemistry*, **34**, 255.
45. J. Stumper, S. A. Campbell, D. P. Wilkinson, M. C. Johnson, and M. Davis, *Electrochimica Acta*, **43**, 3773 (1998).
46. Y.-G. Yoon, W.-Y. Lee, T.-H. Yang, G.-G. Park, and C.-S. Kim, *Journal of Power Sources*, **118**, 193 (2003).
47. T. Mennola, M. Noponen, M. Aronniemi, T. Hottinen, M. Mikkola, O. Himanen, and P. Lund, *Journal of Applied Electrochemistry*, **33**, 979 (2003).
48. M. Noponen, T. Mennola, M. Mikkola, T. Hottinen, and P. Lund, *Journal of Power Sources*, **106**, 304 (2002).
49. S. Ladre, O. E. Kongstein, A. Oedegaard, F. Seland, and H. Karoliussen, *ECS Transactions*, **50**, 829 (2013).
50. U.S. Department of Energy, *Fuel Cell Technologies Office Multi-Year Research, Development, and Demonstration Plan*, in, p. 29 (2012).
51. M. Pourbaix, *Atlas of electrochemical equilibria in aqueous solutions*, Pergamon Press, Oxford; New York (1966).
52. G. Hinds and E. Brightman, *International Journal of Hydrogen Energy*, **40**, 2785 (2015).